MRI Contrast Agents

DOI: 10.1002/anie.200905133

Gadolinium-Conjugated Dendrimer Nanoclusters as a Tumor-Targeted T_1 Magnetic Resonance Imaging Contrast Agent**

*Zhiliang Cheng, Daniel L. J. Thorek, and Andrew Tsourkas**

Contrast agents are being used increasingly in diagnostic magnetic resonance (MR) imaging to help detect and characterize pathological abnormalities. In fact, it has been estimated that nearly 50% of all MR examinations already involve the use of MR contrast agents, with chelated gadolinium compounds being by far the most widely used.[1,2] Most clinically relevant gadolinium-based agents are small, non-targeted compounds that passively distribute into the intravascular and interstitial space.[3] However, there has recently been emerging interest in the development of paramagnetic contrast agents that are capable of probing the molecular profile of tissues by ligand targeting, enzymatic activity, and multiplexing.[4,5] It is envisioned that these agents could be used to acquire a more specific clinical diagnosis and thus improve patient management.

To compensate for the low signal enhancement generated by individual gadolinium ions, most targeted gadolinium compounds have relied on the development of nanoplatforms that can carry a high payload of gadolinium and enhance the longitudinal relaxivities (R_1) per gadolinium. A wide range of macromolecules and other nanoparticulate systems have already been tested as platforms for gadolinium labeling, including dendrimers,[6–12] polymers,[13] emulsions,[14] silica nanoparticles,[15–17] and vesicles.[18–21] Some of these agents have relaxivities on the order of 10^5 to 10^6 $mM^{-1}s^{-1}$ per nanoparticle.[14,17,18] As the R_1 value for chelated gadolinium is typically only between 5 and 30 $mM^{-1}s^{-1}$ when attached to these nanoparticulate carriers, these contrast agents clearly benefited most from their ability to carry a high gadolinium payload. Furthermore, as the theoretical maximum R_1 for gadolinium is estimated to be only about 80 $mM^{-1}s^{-1}$ (1.5 T),[22] it can be argued that any major future improvements in the R_1 value per particle will be achieved through the development of nanoplatforms that support higher gadolinium payloads. Considering that most current nanoplatforms are only labeled with gadolinium chelates on their outer surface, to ensure high water accessibility, we hypothesized that higher gadolinium payloads could be achieved by the development of highly porous nanoparticles that contained a high gadolinium content throughout the intraparticular volume. Herein, we show that this could be accomplished by creating dendrimer nanoclusters (DNCs) composed of individual gadolinium-labeled PAMAM dendrimers that have been cross-linked to form larger nanoparticulate carriers. We also demonstrate that these gadolinium-labeled DNCs can readily be functionalized with targeting ligands (e.g. folic acid) and used for in vivo molecular imaging. The synthesis of a folate-receptor targeted gadolinium-labeled DNC is shown in Figure 1.

Paramagnetic DNCs were prepared by first crosslinking fifth-generation PAMAM dendrimers with the homobifunctional amine-reactive crosslinking agent NHS-PEG-NHS. The presence of a polyethylene glycol (PEG) spacer arm helped maintain the high water solubility of the formed dendrimer clusters. To control nanocluster size, the molar ratio between NH_2-containing PAMAM dendrimer and NHS-containing $BS(PEG)_5$ cross-linker was varied. It was found that at a molar ratio of 50:1 [NH_2]:[NHS] it was possible to obtain DNCs with an average hydrodynamic diameter of 150 nm and a relatively narrow size distribution, as determined by dynamic light scattering (DLS) measurements (see Supporting Information, Figure S1A). Non-crosslinked individual dendrimers, with an average diameter of 5.8 nm, were removed by repeated washes on a 100 nm centrifugal filter device. The purified DNCs were labeled with gadolinium by reacting the amine functional groups with the chelating agent diethylenetriaminopentaacetic acid (DTPA) dianhydride. The resulting paramagnetic DNCs were further functionalized with the optical imaging dye fluorescein isothiocyanate (FITC) and the tumor-targeting ligand folic acid.

Transmission electron microscopy (TEM) confirmed the labeling of the DNCs with gadolinium (see Supporting Information, Figure S1B). Owing to the presence of the electron-dense gadolinium ions, DNCs were directly placed on a carbon-coated copper grid and observed without using any additional staining agents that are often required to enhance the contrast of unmodified dendrimers.[23] The DNCs observed by TEM were approximately spherical in shape and 75–150 nm in diameter. These values are slightly smaller than the size measurements acquired by DLS and may reflect the difference between the hydrodynamic diameter measured by DLS and the physical diameter measured by TEM. The smaller average DNC size, based on TEM measurements, could also be a consequence of the limited number of DNCs analyzed in TEM micrographs ($n = 20$).

To assess the paramagnetic properties of the gadolinium-conjugated DNCs, the amount of gadolinium within the

[*] Dr. Z. Cheng, D. L. J. Thorek, Dr. A. Tsourkas
Department of Bioengineering, University of Pennsylvania
210 South 33rd Street, 240 Skirkanich Hall
Philadelphia, PA 19104 (USA)
Fax: (+1) 215-573-2071
E-mail: atsourk@seas.upenn.edu

[**] This work was supported in part by the National Institute of Health (NCI) R21 CA-132658 and the American Cancer Society RSG-07-005-01.

Supporting information for this article, including detailed experimental procedures, materials used, DLS/TEM measurements, cellular uptake, cell pellets, and cell viability, is available on the WWW under http://dx.doi.org/10.1002/anie.200905133.

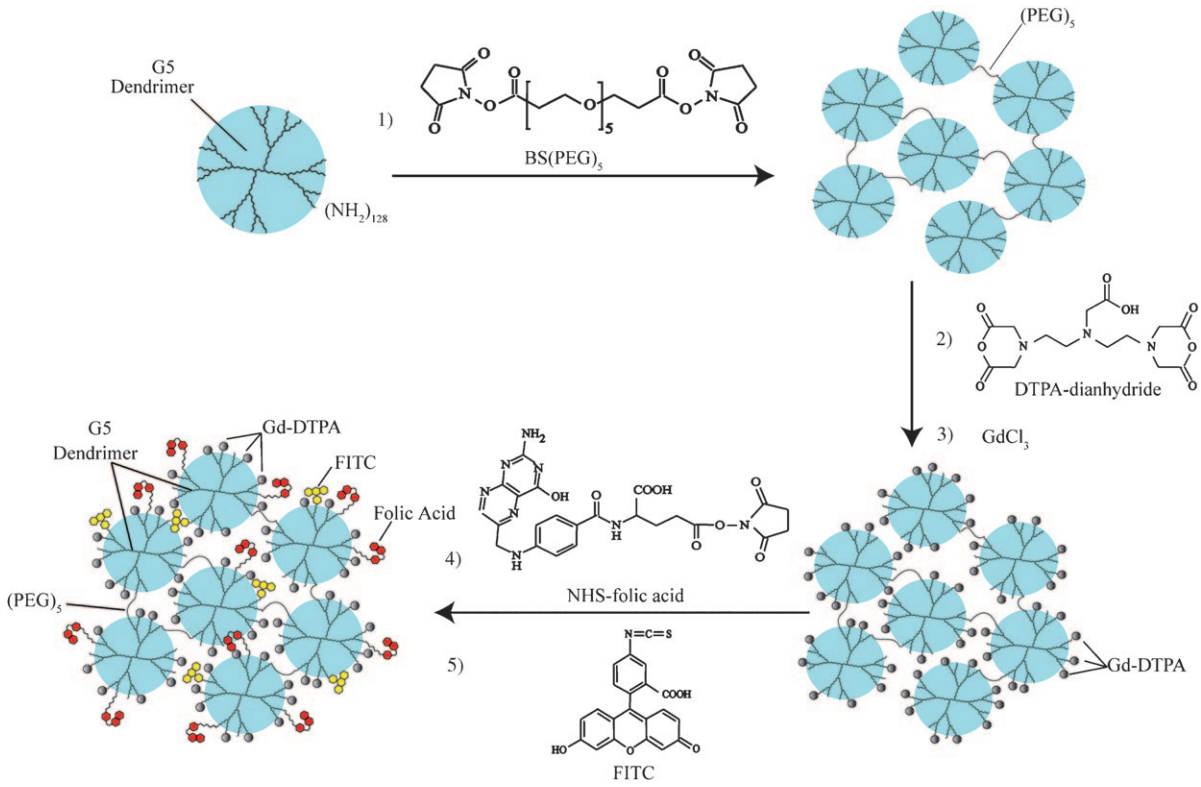

Figure 1. Paramagnetic targeted dendrimer nanoclusters (DNCs). Nanoclusters were fabricated by crosslinking polyamidoamine (PAMAM) fifth-generation dendrimers using a bifunctional amine-reactive crosslinker (1). Following DNC formation, paramagnetic Gd^{3+} ions were conjugated to DNCs by DTPA (2,3). The resulting paramagnetic DNCs were further functionalized with the tumor-targeting ligand folic acid (4) and the fluorescence dye FITC (5).

sample was determined by inductively coupled plasma atomic emission spectroscopy (ICP-AES). The relaxivity was then calculated as the slope of the curves $1/T_1$ versus gadolinium concentration (Figure 2). T_1 relaxation times were determined using a Bruker mq60 MR relaxometer operating at 1.41 T (60 MHz) and at 40 °C. Gadolinium-conjugated DNCs had an R_1 relaxivity value of 12.3 $mM^{-1}s^{-1}$ per gadolinium atom. This value was only slightly higher than gadolinium-labeled individual PAMAM (G5) dendrimers, which had an R_1 relaxivity of 10.1 $mM^{-1}s^{-1}$ per gadolinium atom. It is likely that only a marginal increase in R_1 was observed, despite the larger size of DNCs, owing to a large amount of internal motion within the DNCs caused by the PEG linkers. Saturation of ion relaxivity, which has previously been reported for high-generation dendrimers, could also be a contributing factor.[24] As a point of comparison, Gd-DTPA was determined to have an R_1 of 3.9 $mM^{-1}s^{-1}$ per gadolinium.

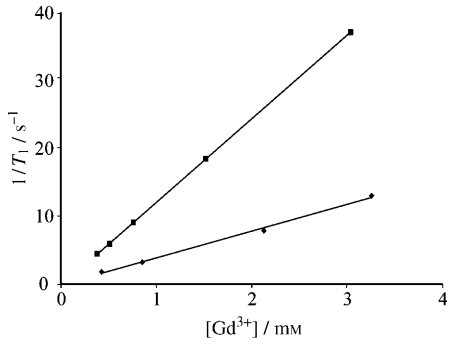

Figure 2. Relaxivity (R_1) measurements for gadolinium-labeled DNCs (■, $R_1 = 12.3$ $mM^{-1}s^{-1}$) and Gd-DTPA (◆, $R_1 = 3.9$ $mM^{-1}s^{-1}$).

To determine the R_1 per DNC particle, it was first necessary to determine the number of particles within a given aqueous sample. This was accomplished by using Einstein's viscosity equation to determine the volume fraction of the DNCs and DLS measurements to determine the average volume of individual DNCs.[25] Subsequent measurements of gadolinium content in the same samples by ICP-AES revealed that there were approximately 300000 Gd per DNC. For comparison, individual fifth-generation dendrimers possess a maximum of 128 functional groups for attachment of single gadolinium chelates. Higher-generation dendrimers can, of course, be used to carry higher payloads, but these dendrimers are difficult to synthesize and costly. Furthermore, even a tenth-generation dendrimer can only accommodate a maximum of 4096 single gadolinium chelates.[24] Accordingly, gadolinium payloads are typically reported to be in the range of 4 to 1860 Gd per dendrimer.[8,24] The dramatic difference in gadolinium payload between DNCs and individual dendrimers arises from both the larger size of the DNCs and the ability of DNCs to carry chelated gadolinium throughout the intraparticular volume, and not just on its

outer shell. Based on the average gadolinium content of each DNC and the relaxivity per gadolinium, it is estimated that the relaxivity per DNC is approximately 3.6×10^6 mM^{-1}s^{-1}.

The paramagnetic properties of the DNCs reported herein compare very favorably with gadolinium-based agents that have previously been reported. For example, gadolinium-labeled shell-crosslinked nanoparticles (40 nm diameter) have an R_1 value of 39 mM^{-1}s^{-1} per Gd (0.47 *T*) but possess only 510 gadolinium atoms per particle, which results in an R_1 of 2×10^4 mM^{-1}s^{-1} per nanoparticle.[26] Paramagnetic silica nanoparticles (ca. 100 nm) have an R_1 of 9.0 mM^{-1}s^{-1} per Gd (4.7 *T*) and contain 16000 Gd per nanoparticle, which results in an R_1 of 1.4×10^5 mM^{-1}s^{-1} per nanoparticle.[17] Gadolinium-encapsulated porous polymersomes (ca. 125 nm) possess nearly 44000 Gd per particle and exhibit an R_1 of 3.2×10^5 mM^{-1}s^{-1} per nanoparticle.[18] Consequently, all three of these particle types exhibit relaxivities that are significantly lower than the paramagnetic DNCs presented herein.

Perfluorocarbon nanoparticles have a reported R_1 value of 25.3 mM^{-1}s^{-1} per Gd (1.5 *T*) and 94200 Gd per particle, which results in an R_1 of 2.38×10^6 mM^{-1}s^{-1} per nanoparticle;[14] however, whilst this relaxivity is similar to that of the 150 nm DNCs, it should be noted that the perfluorocarbon particles are much larger, with a diameter of 273 nm. Scaling with volume, a paramagnetic DNC of this size would possess 1800000 Gd and exhibit an R_1 of 2.2×10^7 mM^{-1}s^{-1}.

To confirm the folate-receptor-targeting capabilities of the DNCs, KB cells were incubated with DNCs for two hours and subsequently analyzed by fluorescence microscopy. KB cells are known to express the folate receptor, and they are often used as a model cell line to evaluate the targeting capabilities of folic acid-labeled nanoparticles. All of the DNCs were labeled with FITC, along with folic acid and Gd-DTPA. Indicative of cell labeling, all of the KB cells exhibited a bright fluorescent signal (Figure 3). To verify that uptake of the DNCs was mediated through folate-receptor-dependent targeting; competitive inhibition studies were conducted by adding DNCs to cell cultures in the presence of excess free folic acid. Under these conditions, fluorescence was significantly reduced. Moreover, when folate-targeted DNCs were incubated with NIH 3T3 cells, which are negative for the folate receptor, very little cellular fluorescence was observed (see Supporting Information, Figure S2). These findings confirm that cellular binding of DNCs was specifically mediated by the folate receptor.

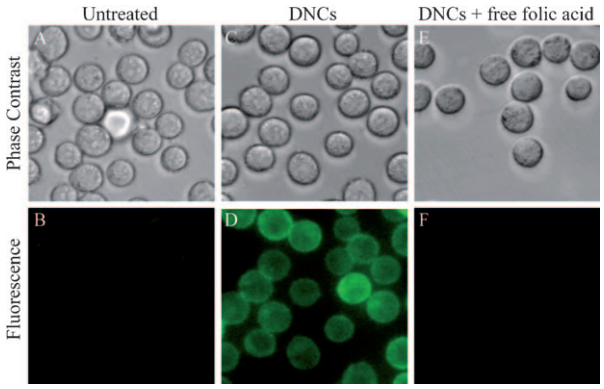

Figure 3. Cellular uptake of fluorescently labeled DNCs. A,B) Phase contrast and fluorescent images of untreated KB cells, and C,D) KB cells following 2 h incubation with FITC-labeled DNCs. The DNCs are also labeled with folic acid and Gd-DTPA. E,F) KB cells following 2 h incubation with FITC-labeled DNCs in the presence of 5 mM free folic acid.

Cell labeling with DNCs was further assessed by acquiring T_1-weighted magnetic resonance (MR) images of KB cells that were pelleted in PCR tubes, following incubation with DNCs in the presence and absence of free folic acid (see Supporting Information, Figure S3). KB cells that were incubated with DNCs alone exhibited a significant enhancement in MR signal intensity compared with unlabeled cells. Conversely, cells that had been incubated with DNCs in the presence of excess free folic acid only showed a slight increase in signal intensity, indicating that the free folic acid was able to specifically block the binding of the DNCs. These results further confirm that DNCs can efficiently bind KB cells by the folate receptor.

Prior to evaluating DNCs in living subjects, cytotoxic effects of DNCs were examined in a MTT cell proliferation assay (MTT = 3-(4,5-dimethylthiazol-2-yl)2,5-diphenyl-tetrazoilum bromide). Specifically, various concentrations of the folate-receptor-targeted DNCs were incubated with KB cells, which are known to express the folate receptor, and NIH 3T3 cells which do not, for 24 h. The data indicate the cell viabilities for each cell type normalized to a control cell sample that was not incubated with any DNCs (see Supporting Information, Figure S4). In general, DNCs had little effect on the viability of NIH 3T3 cells up to a gadolinium concentration of 5 mM (i.e., about 90% viability). However, gadolinium concentrations of 0.1 mM and above did appear to have an effect on the viability of KB cells, with viability falling to about 66% at gadolinium concentrations of 5 mM. It is suspected that the observed level of KB cell death is attributable to the high driving force for cell internalization imparted by the folic acid on the DNCs and the long incubation time (24 h).

To examine whether DNCs could be used to effectively identify folate-positive tumors in living subjects, axial MR images of mice with subcutaneous KB cell xenografts were acquired precontrast and at various times after intravenous (i.v.) injection of DNCs (0.3 mmol Gd/kg) (Figure 4). In the precontrast images, there was little intrinsic contrast between the implanted KB tumors and surrounding muscle. At one hour following administration of the DNCs, a slight contrast enhancement was observed within the KB tumor. The signal enhancement increased significantly by 4 h, and by 24 h the signal within the tumor was extremely bright and the boundary of the tumor was clearly demarcated.

Control experiments to assess specificity were performed by i.v. injection of DNCs in the presence of free folic acid (50 mM), into mice with subcutaneous KB cell xenografts. In these animals, a slight enhancement in signal within the tumor was observed; however, the signal was clearly lower than when DNCs were administered alone for each of the time points studied. Similarly, when DNCs were injected into mice with folate-receptor-negative tumors (i.e., subcutaneous T6-

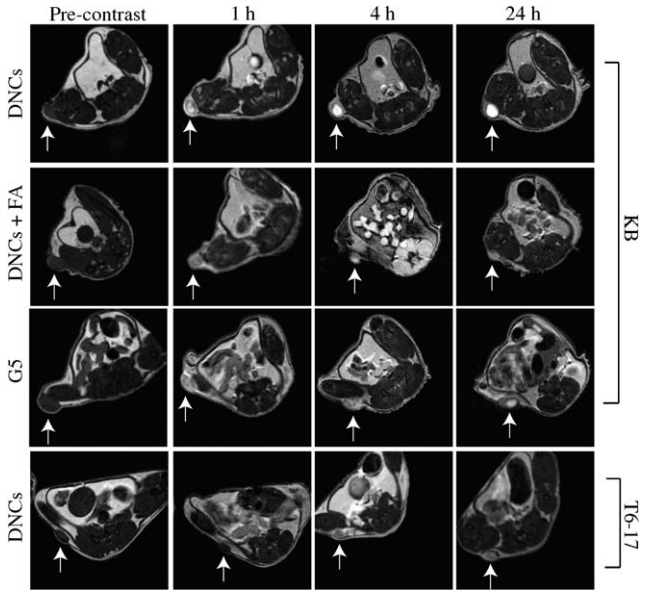

Figure 4. MR images of nude mice with subcutaneous tumor xenografts at various timepoints following the intravenous (i.v.) injection of gadolinium-labeled nanoparticles. The local hyperintensity generated by the gadolinium-labeled nanoparticles was visualized using a 4.7 *T* small-animal MR. Top row: mice with KB cell tumor xenografts before and after i.v. injection with folate receptor-targeted DNCs. Second row: mice with KB cell tumor xenografts before and after i.v. injection with folate receptor-targeted DNCs in the presence 50 mM free folic acid (FA). Third row: mice with KB cell tumor xenografts before and after i.v. injection with folate receptor-targeted, gadolinium-labeled dendrimers (individual fifth-generation dendrimers). Fourth row: mice with T6-17 cell tumor xenografts (i.e. folate receptor-negative) before and after i.v. injection with folate receptor-targeted DNCs. Images were acquired pre-injection and 1, 4 and 24 h post-injection; white arrow shows location of tumor.

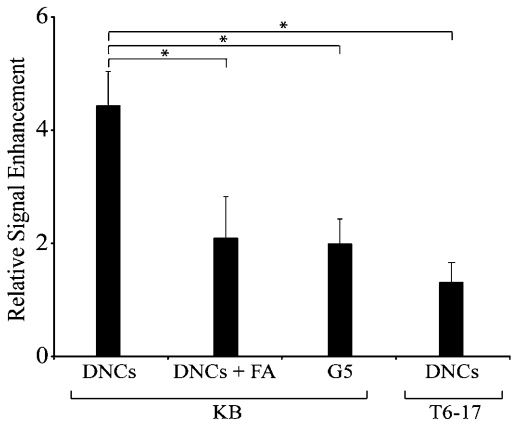

Figure 5. Quantitative analysis of MR images. The average MR signal intensity was measured for each tumor and the relative signal enhancement, rSE, was then calculated as the quotient of the intensity in the 24 h post-contrast image and the pre-contrast image. A *t*-test (two-tailed, unequal variance) was used to compare the rSE for each group of animals. A $p < 0.05$ was considered statistically significant and is indicated by an asterisk.

17 cell xenografts), very little enhancement in contrast was observed between pre- and postcontrast images. As an additional control, we also compared the signal enhancement of DNCs to gadolinium-labeled G5 dendrimers, which were also functionalized with folic acid and administered at the same gadolinium dose. In agreement with previous reports, the targeted dendrimers did exhibit a slight enhancement in signal within the KB tumor compared the precontrast images; however, the signal was noticeably lower than that observed with DNCs. Quantitative analysis of the MR images is presented in Figure 5. These results confirm that the presence of free folic acid led a statistically significant reduction in DNC binding to KB tumor cells ($p < 0.05$), confirming the specificity of the folate-receptor targeting. The residual signal that was observed even in the presence of folic acid (i.e., relative signal enhancement of greater than unity) is suspected to be due to incomplete blocking of the folate receptor (especially considering the rapid clearance of free folic acid) and because of the enhanced permeability and retention effect within the KB tumor. Analysis of the MR images also revealed that DNCs exhibited a statistically significant improvement in image contrast compared with targeted dendrimers ($p < 0.05$).

In conclusion, we have provided a facile method for the synthesis of nanometer-sized dendrimer nanoclusters. Owing to the many chemically functional amine groups present within DNCs, a high capacity for gadolinium labeling was achieved by simple and efficient DTPA chelation. Furthermore, we have demonstrated the utility of these DNCs as optical and MR imaging contrast agents for the in vitro and in vivo detection of tumor cells overexpressing the folate receptor. By conjugating appropriate cancer-targeting ligands, the ultrasensitive MR detection of various types of cancers may be possible. Therefore, we believe that the DNCs described herein provide a powerful new platform for the early detection of disease. Of course, before any new gadolinium-based contrast can be extended to the clinic, their toxicological profile must be carefully evaluated, especially with the increasing concerns over gadolinium-mediated toxicity, such as nephrogenic systemic fibrosis. This point is particularly relevant for gadolinium-labeled nanoparticles, which generally exhibit longer circulation and residence times compared with chelated gadolinium. As a consequence, future work will be aimed at developing biodegradable dendrimers and/or crosslinkers that can be eliminated from the body in a reasonable period of time after carrying out their diagnostic function. Efforts will also be made to reduce the size distribution of the DNCs. It is likely that DNCs within the reported population exhibited size-dependent variability in their retention, biodistribution, and mechanism of nanoparticle uptake. In general, it is preferable to have a more monodisperse sample with uniform pharmacokinetics.

Received: September 14, 2009
Revised: October 20, 2009
Published online: December 3, 2009

Keywords: dendrimers · gadolinium · imaging agents · magnetic resonance imaging · tumors

[1] M. F. Bellin, *Eur. J. Radiol.* **2006**, *60*, 314 – 323.
[2] F. G. Shellock, E. Kanal, *JMRI-J. Magn. Reson. Imaging* **1999**, *10*, 477 – 484.
[3] P. Caravan, J. J. Ellison, T. J. McMurry, R. B. Lauffer, *Chem. Rev.* **1999**, *99*, 2293 – 2352.
[4] J. L. Major, T. J. Meade, *Acc. Chem. Res.* **2009**, *42*, 893 – 903.
[5] Y. Song, E. K. Kohlmeir, T. J. Meade, *J. Am. Chem. Soc.* **2008**, *130*, 6662 – 6663.
[6] C. A. Boswell, P. K. Eck, C. A. S. Regino, M. Bernardo, K. J. Wong, D. E. Milenic, P. L. Choyke, M. W. Brechbiel, *Mol. Pharm.* **2008**, *5*, 527 – 539.
[7] H. Kobayashi, M. W. Brechbiel, *Adv. Drug Delivery Rev.* **2005**, *57*, 2271 – 2286.
[8] S. Langereis, Q. G. de Lussanet, M. H. P. van Genderen, E. W. Meijer, R. G. H. Beets-Tan, A. W. Griffioen, J. M. A. van Engelshoven, W. H. Backes, *NMR Biomed.* **2006**, *19*, 133 – 141.
[9] S. Langereis, A. Dirksen, T. M. Hackeng, M. H. P. van Genderen, E. W. Meijer, *New J. Chem.* **2007**, *31*, 1152 – 1160.
[10] J. Rudovský, M. Botta, P. Hermann, K. I. Hardcastle, I. Lukes, S. Aime, *Bioconjugate Chem.* **2006**, *17*, 975 – 987.
[11] S. D. Swanson, J. F. Kukowska-Latallo, A. K. Patri, C. Y. Chen, S. Ge, Z. Y. Cao, A. Kotlyar, A. T. East, J. R. Baker, *Int. J. Nanomed.* **2008**, *3*, 201 – 210.
[12] W. L. Zhu, B. Mollie, Z. M. Bhujwalla, D. Artemov, *Magn. Reson. Med.* **2008**, *59*, 679 – 685.
[13] M. G. Duarte, M. H. Gil, J. A. Peters, J. M. Colet, L. Vander Elst, R. N. Muller, C. Geraldes, *Bioconjugate Chem.* **2001**, *12*, 170 – 177.
[14] A. M. Morawski, P. M. Winter, K. C. Crowder, S. D. Caruthers, R. W. Fuhrhop, M. J. Scott, J. D. Robertson, D. R. Abendschein, G. M. Lanza, S. A. Wickline, *Magn. Reson. Med.* **2004**, *51*, 480 – 486.
[15] Y. S. Lin, Y. Hung, J. K. Su, R. Lee, C. Chang, M. L. Lin, C. Y. Mou, *J. Phys. Chem. B* **2004**, *108*, 15608 – 15611.
[16] W. J. Rieter, J. S. Kim, K. M. L. Taylor, H. Y. An, W. L. Lin, T. Tarrant, W. B. Lin, *Angew. Chem.* **2007**, *119*, 3754 – 3756; *Angew. Chem. Int. Ed.* **2007**, *46*, 3680 – 3682.
[17] S. Santra, R. P. Bagwe, D. Dutta, J. T. Stanley, G. A. Walter, W. Tan, B. M. Moudgil, R. A. Mericle, *Adv. Mater.* **2005**, *17*, 2165 – 2169.
[18] Z. L. Cheng, A. Tsourkas, *Langmuir* **2008**, *24*, 8169 – 8173.
[19] S. Hak, H. Sanders, P. Agrawal, S. Langereis, H. Grull, H. M. Keizer, F. Arena, E. Terreno, G. J. Strijkers, K. Nicolay, *Eur. J. Pharm. Biopharm.* **2009**, *72*, 397 – 404.
[20] E. Terreno, D. D. Castelli, C. Cabella, W. Dastru, A. Sanino, J. Stancanello, L. Tei, S. Aime, *Chem. Biodiversity* **2008**, *5*, 1901 – 1912.
[21] E. C. Unger, P. Macdougall, P. Cullis, C. Tilcock, *Magn. Reson. Imaging* **1989**, *7*, 417 – 423.
[22] P. Caravan, C. T. Farrar, L. Frullano, R. Uppal, *Contrast Media Mol. Imaging* **2009**, *4*, 89 – 100.
[23] C. L. Jackson, H. D. Chanzy, F. P. Booy, B. J. Drake, D. A. Tomalia, B. J. Bauer, E. J. Amis, *Macromolecules* **1998**, *31*, 6259 – 6265.
[24] L. H. Bryant, M. W. Brechbiel, C. C. Wu, J. W. M. Bulte, V. Herynek, J. A. Frank, *JMRI-J. Magn. Reson. Imaging* **1999**, *9*, 348 – 352.
[25] F. Reynolds, T. O'Loughlin, R. Weissleder, L. Josephson, *Anal. Chem.* **2005**, *77*, 814 – 817.
[26] J. L. Turner, D. P. J. Pan, R. Plummer, Z. Y. Chen, A. K. Whittaker, K. L. Wooley, *Adv. Funct. Mater.* **2005**, *15*, 1248 – 1254.

